Analytical Methods

Accepted Manuscript

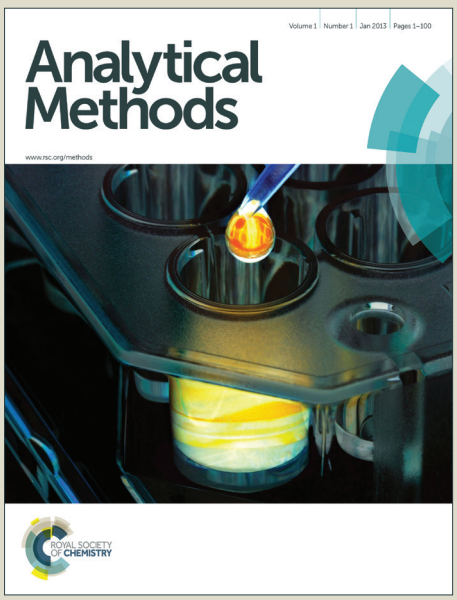

ROYAL SOCIETY OF CHEMISTRY

www.rsc.org/methods

Direct electrochemistry and bioelectrocatalysis of horseradish peroxidase entrapped in a self-supporting nanoporous gold electrode: a new strategy to improve the orientation of immobilized enzyme

Lu Lu,*[ab] Yanjie Dong,[a] Junwei Wang,[a] Qianqian Li[a] and Xia Wu*[a]

[a]*School of Chemistry and Chemical Engineering, Anqing Normal University, Anqing 246011, P. R. China*

[b]*Collaborative Innovation Center for Petrochemical New Materials, Anqing 246011, P. R. China*

*Corresponding author: Lu Lu and Xia Wu

Address: No. 128 Linghu Nanlu

Anqing Normal University

School of Chemistry and Chemical Engineering

Anqing 246011, China

Tel.: +86-556-550-0090; Fax: +86-556-550-0090

E-mail address: lulu19861117@126.com; xiawu@aqtc.edu.cn

Abstract

The single redox active center (heme) is located deeply and asymmetrically in horseradish peroxidase (HRP), leading to a low direct electron transfer efficiency of HRP with random orientation on plane electrodes. To improve its orientation and availability, HRP was attempted to be embedded in a porous material in this study, benefiting from the encapsulation of nanopores. A self-supporting nanoporous gold electrode (NPGE) was preferred and first prepared in a water/air-stable ionic liquid ([Choline]Cl $2ZnCl_2$) using electrochemical alloying/dealloying method. To obtain suitable pores for HRP, the effect of temperature, which was a key factor for the formation of Au-Zn alloy, on the morphology of NPGE was investigated, realizing the temperature control for the pore size. The direct electrochemistry and bioelectrocatalysis of HRP embedded in the suitable nanopores were investigated detailedly. The proportion of the enzyme molecules with effective direct electron transfer was as high as 85.8% of the total amount of the immobilized HRP. The apparent electron transfer rate constant was calculated to be (2.04 ± 0.12) s^{-1}. This biosensor displayed an excellent and rapid electrocatalytic response to H_2O_2 at a low overpotential with the linear range of 10-380 μM, the sensitivity of 21 μA mM^{-1} and the detection limit of 2.6 μM (S/N=3), and it possessed good stability, reproducibility and selectivity for H_2O_2. This easy but effective strategy not only favors for improving the orientation of HRP in nanopores, but also takes advantage of the electron acceleration of the nano-ligaments of NPG, expanding the application field of NPG in electrochemical biosensors.

Keywords: Horseradish peroxidase; Orientation; Direct electron transfer; Nanoporous gold; Ionic liquid

Introduction

The efficient direct electron transfer (DET) between redox proteins and electrodes is significant for understanding the electron transfer process in biological systems and the development of the third-generation biosensor. Horseradish peroxidase (HRP), which is a typical heme-containing oxidoreductase, is usually used as a model to investigate the DET process due to its explicit electron transfer mechanism and important application for the catalytic oxidation of many peroxides.[1,2] It can be seen from the HRP structure that 1) the electroactive center buries deeply in the enzyme molecule, leading to the difficult DET on plane electrodes; 2) the electroactive center is located asymmetrically in the HRP, so the enzyme molecules with active center near the electrode surface are easier for the DET. Therefore, the unfavorable orientation of the enzyme molecules is the main reason for the low DET efficiency at plane electrodes. The recombinant HRP based on biological modification with the favorable orientation immobilized on the electrode surface is a good strategy to enhance the DET efficiency.[3-5] But the operating steps are very complicated. In this work, the orientation of HRP molecules is attempted to be improved from the new perspective of the electrode material, *i.e.*, the HRP molecules are embedded in porous electrode so that the DET is much easier even if their orientation is random. Compared with the easily aggregating gold nanoparticles, nanoporous gold (NPG) is a bulk material composed of nano-sized pores and ligaments.[6,7] These pores provide a favorable environment for immobilizing HRP and its DET, and the wormlike ligaments can facilitate the DET. In addition, NPG with large surface area is conductive, chemically and mechanically stable and biocompatible, becoming an attractive material for immobilizing enzymes and constructing the electrochemical biosensors.[8]

At present, dealloying method for NPG preparation is widely recognized. An alloy is usually obtained by melting Au and Ag in appropriate proportions, and NPG is then prepared by

removing Ag in concentrated nitric acid.[6,9] In addition to the high-temperature conditions for preparing the alloy, the NPG thin film is usually needed to be adhered to the substrate electrode surface because it is hard to be used as a self-supporting electrode. As a result, the preparation procedure of an enzyme-NPG electrode is relatively complicated and the electron transfer is adversely affected due to the poor contact between the NPG film and the substrate electrode.[10] Recently, the self-supporting NPG electrode (NPGE) was fabricated via cyclic voltammetry (CV), which is an effective in-situ electrochemical alloying/dealloying method, at *ca.* 120 ℃ using benzyl alcohol[11,12] or dimethyl sulfoxide[13] as the medium, avoiding the use of hazardous cyanides and bases or acids. In this way, a more facile method with ethylene glycol as the medium was also developed to fabricate NPGE in our previous work.[14] Compared with the traditional organic solvents, "green" solvents ionic liquids (ILs) have been attracted much attention and interest due to their high conductivity, wide electrochemical window, good thermal stability and negligible vapor pressure.[15] And ILs have been proven to be suitable electrolytes for electrodeposition. Using [1-ethyl-3-methylimidazolium]Cl·$ZnCl_2$ (2:3) as the medium, NPG,[15-17] porous silver[18] and nanopatterning palladium[19] were fabricated via electrochemical alloying/dealloying method. As reported, the preparation processes of NPG needed to be carried out in a glove box to avoid the moisture absorption or metamorphism of this IL.[15] As one of the novel Lewis acid ILs, in addition to the above excellent properties, [Choline]Cl·x$ZnCl_2$ is water/air stable and low-cost compared with imidozalium-based ILs.[20-22] It provides a wide working temperature and is a good candidate as the medium for fabricating the self-supporting NPGE.

In this work, a self-supporting NPGE with proper pores for immobilizing HRP and large surface area is first fabricated in Lewis acid [Choline]Cl·2$ZnCl_2$ via in-situ electrochemical alloying/dealloying method. Then an electrochemical biosensor is constructed by embedding HRP in NPGE. The direct electrochemistry and bioelectrocatalysis of HRP are investigated detailedly. The electron transfer efficiency of HRP will be increased due to the improvement of

the orientation of enzyme molecules, the large surface area of NPGE and the electronic promotion of the nano-sized ligaments. This study not only provides scientific support for understanding the promoting mechanism of the DET, but also expands the application of NPG in electrochemical biosensors.

Experimental

Materials and instruments

Ionic liquid [Choline]Cl (99.9%) was provided by Shanghai Chengjie Chemicals Co. Ltd. and used without further purification. HRP (EC 1.11.1.7, 250 U mg^{-1}), $ZnCl_2$ (A. R.), $K_3[Fe(CN)_6]$ (A. R.), $K_4[Fe(CN)_6]$ (A. R.), KCl (A. R.) and *o*-phenylenediamine (OPD, A. R.) were purchased from Sinopharm Chemical Reagent Co. Ltd. Gold wire with 99.999% purity (0.5 mm in diameter), Zinc wire and Zinc plate were provided by Tianjin Aidahengsheng Technology Co. Ltd. H_2O_2 (A. R., 30 wt.%) was purchased from Tianjin Bodi Chemical Industry Stock Co. Ltd. Phosphate buffer (0.1 M, pH 7.0) was prepared by mixing stock standard solutions of Na_2HPO_4 and NaH_2PO_4 and adjusting the pH with 0.1 M H_3PO_4 or NaOH. All other reagents were of analytical grade and used as received. Ultrapure water (18.25 MΩ cm) was used throughout the experiments.

All the electrochemical experiments were performed on a CHI 660E Electrochemical Analyser (Shanghai Chenhua Co., China). The surface morphology of the NPGE was characterized with a JEOL JSM-6700F field emission scanning electron microscope (SEM), which was equipped with an Oxford INCA x-sight energy-dispersive X-ray spectrometer (EDS) for compositional analysis. The activity of HRP in the phosphate buffer (pH 7.0) was determined using a UV-visible spectrophotometer (UV-2550, Shimadzu).

Preparation of [Choline]Cl·2$ZnCl_2$

Ionic liquid [Choline]Cl·2$ZnCl_2$ (m.p. 25 ℃) was prepared according to the previous literature.[22] Briefly, a mixture of [Choline]Cl and $ZnCl_2$ in the molar ratio of 1:2 was heated at 100 ℃ in air with gentle stirring until a clear colorless liquid was obtained.

Electrochemical Preparation of NPGEs

The electrochemical fabrication of NPGEs was carried out in [Choline]Cl·2$ZnCl_2$ in one pot without deaerating and special caution. The three-electrode system was composed of a working electrode (gold wire), a counter electrode (Zinc plate) and a reference electrode (Zinc wire). Prior to use, the gold wire was pretreated as follows: first, it was immersed in the freshly prepared Piranha solution (3:1 H_2SO_4 98% : H_2O_2 25%) for 5 min; second, it was polished with 500 nm and 50 nm alumina slurry on chamois leather; finally, the polished wire was cleaned in an ultrasonic cleaner with ethanol and ultrapure water for 5 min, respectively. The geometric area of the gold wire exposed to the ionic liquid was 1.77 mm^2. The CV potential range was -0.4~1.2 V (vs. Zn). When the electrochemical preparation was over, the gold wire was taken out and cleaned with ethanol and ultrapure water respectively. Finally, the gold wire was dried in air.

Preparation of the enzyme electrodes

A freshly prepared NPGE and a smooth gold electrode (SGE) with the same geometric area were immersed in 1.0 mL 2.5 μM HRP solution at 4 ℃ for 24 h, respectively. Then they were rinsed with phosphate buffer (pH 7.0) to remove weakly adsorbed enzyme molecules. The enzyme

electrodes were defined as HRP/NPGE and HRP/SGE. To avoid the leakage of HRP, the enzyme electrodes were covered with Nafion (1.0 wt.%) film, which were defined as Nafion/HRP/NPGE and Nafion/HRP/SGE. When not in use, the aforementioned electrodes were stored at 4 ℃.

Determination of the amount of immobilized HRP

A calibration curve of the initial ratio of enzyme-catalyzed oxidation OPD versus the HRP concentration was first made. Briefly, an aliquot of HRP solution with different concentration was added into the buffer solution (3 mL, pH 7.0) containing 0.3 mM OPD and 0.15 mM H_2O_2. The reaction was monitored immediately by tracing the time dependent change in absorbance at 448 nm. The molar extinction coefficient of the oxidation product of OPD at 448 nm was 10.6 mM^{-1} cm^{-1}.[23] The initial ratio of the oxidation of OPD catalyzed by the residual enzyme in the immobilizing solution was determined (the concentration of HRP in the cuvette was 1/150 of that in the immobilizing solution). Then the concentration of the residual enzyme was obtained from the calibration curve. Finally, the amount of HRP adsorbed on NPGE was calculated based on the difference between the HRP concentration in buffer solution before and after enzyme immobilization. Each activity datum was an average of triplicate measurements with relative deviation less than 5%. The spectroscopic measurement was carried out at *ca.* 25 ℃.

Electrochemical measurements

CV, amperometric and electrochemical impedance spectroscopic (EIS) measurements were performed using the three-electrode system, which was composed of a working electrode (SGE, NPGE or enzyme electrodes), a platinum wire counter electrode and a saturated calomel electrode (SCE) reference electrode. CV and EIS experiments were carried out under quiescent conditions.

The amperometric measurement was made under a hydrodynamic condition. Prior to the measurements, the unmodified gold electrodes were cleaned via repeated scan in H_2SO_4 solution (0.5 M) until reproductive curves were obtained. The electrochemical measurements were carried out at *ca.* 25 ℃.

Results and discussion

Electrochemical alloying/dealloying of gold electrode in [Choline]Cl·2$ZnCl_2$

Fig. 1 shows the fifteenth CV grams of gold electrode in [Choline]Cl·2$ZnCl_2$ at different temperatures. Taking the CV gram at 100 ℃ for example, when the potential moved from +1.2 V toward -0.4 V (vs. Zn), the cathodic peak c_1 (see the inset A) belongs to the under potential deposition peak (UPD) of Zn.[24] The UPD of the metals (such as Zn and Cu) was usually observed at lower scan rates.[25,26] The cathodic peak c_2 belongs to the electrodeposition of the bulk Zn. The onset potential of c_2 was not 0 V but +0.2 V because the porous structure formed previously provided many active sites for the Zn electrodeposition, decreasing the overpotential of the Zn(Ⅱ) reduction.[11] We also observed that the gold surface became silver gradually, further demonstrating Zn was deposited on the gold surface. During the reverse scan, the deposition of Zn continued until 0 V. From 0 V onward, the deposited Zn began to be oxidized. During the subsequent anodic scan, there are two anodic peaks (a_1 and a_2) at +0.52 V and +0.73 V, which are assigned to the bulk Zn and the Zn in alloy, respectively.[11,13] It was observed that the gold surface changed gradually from silver to dark red-brown, indicating that the gold electrode had undergone a whole alloying/dealloying process. Comparatively speaking, the peak potentials of a_1 and a_2 in this IL were more negative than that in benzyl alcohol (ca. +0.85 V and +1.4 V[11]), indicating that the oxidation of the deposited Zn was easier in the present IL. In addition to the

strong coordination between Zn(Ⅱ) and Cl^-, the electrostatic interaction between $[Choline]^+$ and $Zn_aCl_b^-$ should be responsible for the phenomenon. It follows that this IL is a suitable medium for the dealloying process.

Controllability of the NPGE morphology via adjusting temperature

During the electrochemical alloying/dealloying preparation of NPGE, the temperature is the key factor for the formation of Au-Zn alloy. To some extent, the morphology of NPGE depends on the composition of the alloy, which can be controlled by changing the amount of the deposited Zn.[13,15] It is seen from Fig. 1 that the cathodic current increases with the increase of the temperature due to the decrease of the viscosity and the increase of the conductivity of the IL. And the increase magnitude of the cathodic current in the present IL is much bigger than that in the previous solvents[11,13,15] within the same range of the temperature. This is because the change of the viscosity of [Choline]Cl·$2ZnCl_2$ was much bigger with the increase of the temperature.[21] As a result, the amount of the deposited Zn can be controlled conveniently by changing the temperature in the present IL. At 40 ℃ (Fig. S1), only one anodic peak is observed and it is the electrochemical oxidation of the bulk Zn. The SEM image (the inset in Fig. S1) shows a very smooth gold surface, indicating that the Au-Zn alloy was not formed at this low temperature. At 50 ℃, there are two anodic peaks at +0.37 V and +0.50 V (the inset B in Fig. 1), being assigned to the bulk Zn and the Zn in the alloy, respectively. This indicated that the Au-Zn alloy had been readily formed at 50 ℃, which was much lower than that in the organic solvents.[11,13]

The morphology of the gold surface obtained at 50 ℃ was characterized by SEM. Many pores can be observed on this gold surface (Fig. 2A) and some pores are interconnected with each other. With the increase of the temperature, the anodic peak currents of the bulk Zn and the Zn in alloy increase rapidly due to the increase of the amount of the deposited Zn and the alloy at

higher temperatures. It is seen that at the temperatures higher than 50 ℃, the anodic peak potential of Zn in the alloy is much different from that at 50 ℃ due to the formation of the alloy with different compositions probably.[25] Then there are some obvious cracks at 70 ℃ (Fig. 2B). The bicontinuous but not uniform porous structures resulting from the alloying/dealloying process were observed on the gold surface at 90 ℃ (Fig. 2C). When the temperature increased to 100 ℃ (Fig. 2D), the typical and uniform bicontinuous porous structures have been formed. The formation of the porous structure can be explained with the model described by Erlebacher.[27] When the Zn atoms was selectively oxidized from the outermost alloy layer, the residual Au atoms diffused along the alloy/electrolyte interface and agglomerated into some gold-rich islands, exposing new alloy layers to the IL. In the process of the continuous oxidation of Zn and the diffusion of the Au, these gold-rich islands grew to the interconnected porous structure gradually. Compared with the aqueous solutions and organic solvents, the diffusion rate of the Au atoms along the alloy/IL interface became slower due to the bigger viscosity of the IL. However, the dissolution of Zn from the alloy could be facilitated by the strong coordination between Zn(Ⅱ) and Cl^- and the electrostatic interaction between $[Choline]^+$ and $Zn_aCl_b^-$. Therefore the slower diffusion of Au atoms didn't hinder the dissolution of Zn atoms. With the increase of the temperature, the amount of the deposited Zn, the alloy and the diffusion rate of the Au atoms along the alloy/IL interface increased, leading to easier formation of the porous structures. It follows that the effect of the temperature in [Choline]Cl·2$ZnCl_2$ is much bigger than that in aqueous solutions and organic solvents. Then the pore size and depth increase at 110 ℃ (Fig. 2E) and 120 ℃ (Fig. 2F). It was found from the formation mechanism of the porous structure that the dissolution of the inner Zn was more difficult than that of the outer Zn. So with the scan potential becoming more positive via CV, it not only favored for the gradual oxidation of Zn but also prolonged the diffusion time of the Au atoms. The above results indicated that in the present IL,

the temperature was a more crucial factor for the preparation of NPG, which was very important for immobilizing HRP and obtaining good reproducible enzyme electrode. The porosity of the NPGE is a key factor for HRP immobilization, which can be reflected by the electroactive area. For quantitative characterization of the electroactive area of the NPGEs prepared at different temperatures, the CV grams were recorded in 0.5 M H_2SO_4 solution (Fig. S2). The well-defined cathodic peaks at +0.88 V (vs. SCE) resulted from the electroreduction of gold oxide that was formed during the anodic scan.[28] The real area (A_{real}) and roughness factor (R_f), which were estimated based on the charge for the reduction of gold oxide[29] (the conversion factor was 386 μC cm^{-2}),[28] are listed in Table S1. It can be seen that the real area of the NPGE increases with the increase of the alloying/dealloying temperature, which provides the favorable conditions for the subsequent immobilization of more HRP molecules.

Direct electrochemistry of HRP at NPGE

NPGE with suitable pore size for HRP immobilization

The NPGE with suitable pore size and big surface area is crucial for the HRP immobilization. Too big pores may lead to little effect of the pore on the orientation of HRP. In contrast, if the pores are too small, the inner pores can't be used sufficiently, leading to the decrease of the amount of immobilized HRP molecules. The size of an HRP is about 6 nm and our previous results indicated that the NPG or nanoporous cupper with the pore size of 40-50 nm was very suitable for immobilizing laccase[8,30] or HRP.[23] And the comparison of the DET signal (data were not shown here) of HRP in NPGE with different pores (Figs. 2A-2F) indicated that the NPGE with the pore size of 30-50 nm and big surface area (R_f = 42.9) prepared in [Choline]Cl $2ZnCl_2$ at 100 ℃ (Fig. 2D) is suitable for the HRP immobilization. The surface EDS spectrum of the NPGE prepared at 100 ℃ (the inset in Fig. 2D) shows that almost all the Zn atoms were dissolved from

the gold electrode (the amount of residual Zn was 3.76 at.%). It was reported that the proteins immobilized on the unmodified electrode not only reduced the distance between the active center and the electrode surface but also favored for maintaining the native conformation of the proteins.[31,32] It is well accepted that the strong bond can be formed between Au and -S and/or -NH_2.[23] The HRP molecule used here has about eight cysteine, four methionine and seven lysine residues on or near its surface.[23] These amino acid residues can facilitate the multipoint attachment of HRP in NPGE, enhancing the stability of the immobilized enzymes.

EIS characterization of the electrodes

EIS is an effective technique for investigating the interface properties of the modified electrodes. Fig. 3 shows the Nyquist plots of the NPGE (a), HRP/NPGE (b) and Nafion/HRP/NPGE (c) using $[Fe(CN)_6]^{3-/4-}$ as the probe with the frequencies swept from 10^6 to 10^{-3} Hz. The electron transfer resistance, which reflects the interfacial electron transfer ability, can be estimated from the diameter of the semicircle at the region of high frequencies. It is seen that no semicircle was observed in the Nyquist plot of NPGE, indicating a high electron transfer rate at the NPGE due to its good conductivity. However, an obvious semicircle appeared in the Nyquist plot of the HRP/NPGE due to the big resistance of the proteins, demonstrating that the HRP molecules have been immobilized on the NPGE. After being covered with Nation, a bigger semicircle was observed at the Nafion/HRP/NPGE. The resistance was similar to that obtained on the Nafion/Fe_3O_4-Au nanoparticles/HRP electrode and Nafion would not affect the enzymatic electroactivity and catalytic activity.[33]

The DET of HRP at NPGE

Fig. 4 shows the CV grams of Nafion/HRP/SGE (a), NPGE (b) and Nafion/HRP/NPGE (c) in oxygen-free phosphate buffer (0.1 M, pH 7.0). With the range of the potential studied here, no

redox peaks were observed at Nafion/HRP/SGE due to the deep burying of the electroactive center in HRP molecule, the improper orientation of HRP on the SGE and the less amount of immobilized enzyme. As expect, there are no obvious redox peaks at the NPGE, whose background current is much bigger than that of the SGE, resulting from the great increase of the electroactive area of the NPGE. However, a pair of obvious redox peaks is observed at Nafion/HRP/NPGE, indicating that the direct electrochemistry of HRP has been achieved on NPGE. The effective DET was attributed to the unique surface properties of the present NPGE. On one hand, the NPGE with suitable nanopores provided favorable microenviroment for HRP immobilization. The DET of HRP with the heme located asymmetrically was much easier even if their orientation was random, *i.e.*, the orientation of the immobilized enzymes that were surrounded by gold was improved. On the other hand, the surface area of NPGE increased significantly compared with the SGE and more HRP molecules were loaded in NPGE, resulting in the increase of the DET signal. In addition, the wormlike nanoscale ligaments that reduced the distance between the heme and gold, many edge-plane-like defective sites and a good electron-conductive network of NPGE also facilitated the DET.[31] The formal potential ($E^{0'}$) was *ca.* 59 mV, which was more positive than that of some immobilized HRP,[34,35] but close to that of HRP immobilized in (3-mercaptopropyl) trimethoxysilane film (80 mV)[36] and Nafion-cysteine film (60 $\pm$ 4 mV).[37] The redox formal potential of HRP can be affected by the source of the enzyme, the immobilized strategy and the experimental conditions.[38]

To explore the kinetic process of the DET of HRP, the effect of the scan rate on the DET signal was investigated (Fig. 5). It is seen from the inset of Fig. 5 that the redox peak currents increase linearly with the increase of the scan rate (between 0.05 and 0.4 V s^{-1}), indicating that the DET between HRP and NPGE is a typical surface-confined quasi-reversible electrochemical process, further demonstrating that the immobilized HRP in the pores of NPGE is very stable. Based on the integration of the cathodic peak and Faraday's laws, the surface concentration (Γ_c)

of the HRP is estimated according to the following formula:[39]

$$Q = nFA\Gamma_c$$

where Q is total amount of charge quantity of the cathodic reaction, n is the electron transfer number (1), F is the Faraday's constant (96500 C mol^{-1}), and A is the geometric area of the gold electrode. Γ_c was calculated to be 1.94×10^{-9} mol cm^{-2}, which was much bigger than HRP immobilized on gold nanoparticles/3-mercaptopropionic acid/gold electrode (2.4×10^{-10} mol cm^{-2})[34] and CeO_2-reduced grapheme oxide nanocomposite electrode (4.27×10^{-10} mol cm^{-2}).[40] In the most enzyme modified electrodes, the proportion of the enzyme realizing effective DET is usually very low (*ca.* 5%),[41] which leads to the inefficiency of the most immobilized enzymes. In the present work, the concentration of the residual enzyme in the immobilizing solution was obtained from the calibration curve of the initial ratio of HRP-catalyzed oxidation OPD versus HRP concentration (Fig. S3). And then the surface concentration of the adsorbed HRP was calculated to be 2.26×10^{-9} mol cm^{-2}, the proportion of the HRP with effective DET was calculated to be as high as 85.8% due to the improvement of the orientation of the HRP wrapped in the nanopores and the electron promotion of the nanoligaments of NPGE.

It is also seen from Fig. 5 that the redox peak potential changed little with the scan rate ranging from 0.05 to 0.4 V s^{-1}. To obtain the apparent heterogeneous electron transfer rate constant (k_s), the CV behavior of Nafion/HRP/NPGE was investigated at higher scan rates (from 0.5 to 1.0 V s^{-1}). As shown in Fig. S4, when the scan rate was higher than 0.5 V s^{-1}, the redox peak potentials increased with the increase of the scan rate. According to Lavion's methods,[42] we obtained the k_s value of (2.04 ± 0.12) s^{-1}, which was higher than that of HRP immobilized on nanodiamond (1.85 s^{-1}),[43] colloidal gold modified screen-printed electrode (0.75 ± 0.04 s^{-1})[44] and a polystyrene/multiwalled carbon nanotube composite film modified electrode (1.15 s^{-1}),[45] indicating that using NPGE as the substrate favored for the DET of HRP.

Bioelectrocatalysis and amperometric detection of H_2O_2

To explore the bioactivity of the immobilized HRP and the potential application of the Nafion/HRP/NPGE, the bioelectrocatalytic ability of the present enzyme electrode towards H_2O_2 was investigated. As shown in Fig. 6A, with the addition of 0.4 mM H_2O_2, the cathodic peak current increases, while the anodic peak current deceases. This is the characteristics of typical electrocatalytic reduction.[46,47] The cathodic peak potential of the electrocatalytical reduction of H_2O_2 was -0.02 V, which was close to that of the DET of HRP and much more positive than that of H_2O_2 at the bare NPG (-0.4 V vs. SCE[48]), indicating that the bioelectrocatalysis of HRP decreased the overpotential of the reduction of H_2O_2. The above results showed that the bioactivity of the immobilized HRP was maintained and the Nafion/HRP/NPGE had good bioelectrocatalytical ability towards H_2O_2.

To detect H_2O_2 sensitively, the effect of the buffer pH on the electrochemical response of the HRP modified electrode for H_2O_2 was investigated. As shown in Fig. S5, the biggest response current was obtained in the buffer with pH 7.0, which was in accordance with some previous HRP-biosensors.[49-51] Fig. 6B shows a typical amperometric response of the gold wire (a) and Nafion/HRP/NPGE (b) to H_2O_2 at -0.02 V. With the addition of H_2O_2 into the stirred phosphate buffer, the response was hardly observed at the smooth gold wire. Under the same conditions, however, the Nafion/HRP/NPG responded rapidly and a maximum steady-state current was achieved within 5 s. It is seen from the corresponding calibration curve (see the inset) that the response current increases linearly with the increase of the H_2O_2 concentration with the linear range of 10-380 μM, the sensitivity of 21 μA mM^{-1} and the detection limit of 2.6 μM (S/N=3). The comparison of the analytic performance of several HRP biosensors for H_2O_2 determination is listed in Table S2. As is shown, the most immobilized materials are nanoparticles/nanosheets, which are not self-supporting and usually immobilized on other electrodes, leading to some bad

influence of the poor contact between the nanoparticles/nanosheets and the substrate electrode on the electron transfer rate. So the present biosensor shows its advantage for detecting H_2O_2 effectively.

Stability and reproducibility of the H_2O_2 biosensor

The DET signal was relatively stable in phosphate buffer, after ten CV scans, a small change in the cathodic peak current was observed with the relative standard deviation (RSD) of 1.1%. The cathodic peak current was measured every three days and the RSD of five sequential determinations was 3.2%. Three weeks later, the biosensor retained about 89.0% of the initial cathodic peak current. An RSD value of 5.4% in the electrocatalytic current of 0.4 mM H_2O_2 was obtained under the same conditions for four biosensors prepared in the same way, indicating that the reproducibility of the Nafion/HRP/NPGE to H_2O_2 was good.

Anti-interference and real sample analysis of the H_2O_2 biosensor

To investigate the potential application of the biosensor in real detection, the anti-interferential ability of the Nafion/HRP/NPGE was estimated via amperometry. Fig. 7 shows the response current of the biosensor to H_2O_2 and the interferences at -0.02 V in the stirred phosphate buffer. It is seen that with the every addition of H_2O_2, the biosensor responded rapidly. However, the addition of 0.2 mM ascorbic (AA), 0.1 mM glucose and 0.01 mM dopamine (DA) didn't cause obvious current response. These results indicated that the Nafion/HRP/NPGE had good selectivity to H_2O_2.

Since the present biosensor had good stability, reproducibility and selectivity, the real sample analysis for H_2O_2 was carried out. The commercial disinfector containing 3 wt.% H_2O_2 was 5000-

fold diluted with phosphate buffer (0.1 M, pH 7.0) to prepare the sample. The accurate concentration of H_2O_2 could be determined by fluorescence method[52] and the value was 0.168 mM. The results of H_2O_2 determination were listed in Table S3. It can be seen that the recovery was 98.2-103.1%, indicating the present biosensor was feasible to detecting H_2O_2 in real samples.

Conclusions

A self-supporting NPGE with high surface area and suitable nanopores for entrapping HRP molecules was fabricated successfully in water/oxygen-stable [Choline]Cl·$ZnCl_2$ via CV by controlling the temperature. Entrapping HRP in the NPGE resulted in a novel HRP-based biosensor. A large proportion of the enzyme molecules in the NPGE realized their DET. The present biosensor possessed satisfactory detective ability and selectivity towards H_2O_2 oxidation. From the new perspective of the substrate electrode, this strategy improved the disadvantageous orientation of HRP molecules, not only favoring for increasing the proportion of the enzyme molecules with favorable orientation, but also taking advantage of the electron acceleration of the nano-ligaments of NPGE. In this way, a series of biosensors based on the asymmetric single-electroactive-center oxidordeuctases entrapped in self-supporting NPGE with respective suitable nanopores can be developed, expanding the application of NPG in the field of electrochemical biosensor.

Acknowledgments

The authors gratefully acknowledge the financial support from the Scientific Research Foundation of Anqing Normal University (140001000029), National Natural Science Foundation of China (212030022, 21203003) and Anhui Provincial Natural Science Foundation (1308085QB29, 1308085QB44).

References

1. Y. Wang, Z. C. Wang, Y. P. Rui and M. G. Li, *Biosens. Bioelectron.*, 2015, 64, 57-62.
2. Ö. Aybastıer, S. Şahin, E. Işıka and C. Demir, *Anal. Methods*, 2011, **2**, 2289-2297.
3. A. V. Kartashov, G. Serafini, M. D. Dong, S. Shipovskov, I. Gazaryan, F. Besenbachera and E. E. Ferapontova, *Phys. Chem. Chem. Phys.*, 2010, **12**, 10098-10107.
4. E. Ferapontova, V. G. Grigorenko, A. M. Egorov, T. Börchers, T. Ruzgas and L. Gorton, *Biosens. Bioelectron.*, 2001, **16**, 147-157.
5. E. Ferapontova, K. Schmengler, T. Börchers, T. Ruzgas and L. Gorton, *Biosens. Bioelectron.*, 2002, **17**, 953-963.
6. Y. Ding and J. Erlebacher, *J. Am. Chem. Soc.*, 2003, **12**, 7772-7773.
7. H. J. Qiu, Y. L. Sun, X. R. Huang and Y. B. Qu, *Colloids Surf. B: Biointerfaces*, 2010, **79**, 304-308.
8. H. J. Qiu, C. X. Xu, X. R. Huang, Y. Ding, Y. B. Qu and P. J. Gao, *J. Phys. Chem. C*, 2009, **113**, 2521-2525.
9. Y. Ding, Y. Kim and J. Erlebacher, *Adv. Mater.*, 2004, **16**, 1897-1900.
10. F. L. Jia, C. F. Yu, K. J. Deng and L. Z. Zhang, *J. Phys. Chem. C*, 2007, **111**, 8424-8431.
11. F. L. Jia, C. F. Yu, Z. H. Ai and L.Z. Zhang, *Chem. Mater.*, 2007, **19**, 3648-3653.
12. J. H. Jiang and X. Y. Wang, *Electrochem. Commun.*, 2012, **20**, 157-159.
13. H. Dong and X. Cao, *J. Phys. Chem. C*, 2009, **113**, 603-609.
14. L. Lu, X. Huang, Y. Dong, Y. Huang, X. Pan, X. Wang, M. Feng, Y. Luo and D. Fang, *Microchim. Acta*, 2015, **182**, 1509-1517.
15. J. F. Huang and I. W. Sun, *Adv. Funct. Mater.*, 2005, **15**, 989-994.
16. J. Jiang, X. Wang and L. Zhang, *Electrochim. Acta*, 2013, **111**, 114-119.
17. Y. T. Hsieh and I. W. Sun, *Chem. Commun.*, 2014, **50**, 246-248.
18. F. H. Yeh, C. C. Tai, J. F. Huang and I. W. Sun, *J. Phys. Chem. B*, 2006, **110**, 5215-5222.

19. J. Jiang, L. Zhang and X. Wang, *ACS Appl. Mater. Interfaces*, 2013, **5**, 12689-12694.

20. A. P. Abbott, G. Capper, D. L. Davies, H. L. Munro, R. K. Rasheed and V. Tambyrajah, *Chem. Commun.*, 2001, 2010-2011.

21. A. P. Abbott, G. Capper, D. L. Davies and R. K. Rasheed, *Inorg. Chem.*, 2004, **43**, 3447-3452.

22. T. Long, Y. Deng, S. Gan and J. Chen, *Biotechnol. Bioeng.*, 2010, **18**, 322-327.

23. H. J. Qiu, L. Lu, X. R. Huang, Z. H. Zhang and Y. B. Qu, *Bioresour. Technol.*, 2010, **101**, 9415-9420.

24. D. Borissov, A. Pareek, F. U. Renner and M. Rohwerder, *Phys. Chem. Chem. Phys.*, 2010, **12**, 2059-2062.

25. J. Dogel and W. Freyland, *Phys. Chem. Chem. Phys*., 2003, **5**, 2484-2487.

26. P. P. Liu, X. B. Ge, R. Y. Wang, H. Y. Ma and Y. Ding, *Langmuir*, 2009, **25**, 561-567.

27. J. Erlebacher, *J. Electrochem. Soc.*, 2004, **151**, C614-C626.

28. J. H. Jiang and X. Y. Wang, *Electrochem. Commun*., 2012, **20**, 157-539.

29. S. Trasatti and O. A. Petrii, *Pure Appl. Chem.*, 1991, **63**, 711-734.

30. H. J. Qiu, C. X. Xu, X. R. Huang, Y. Ding, Y. B. Qu and P. J. Gao, *J. Phys. Chem. C*, 2008, **112**, 14781-14785.

31. U. Salaj-Kosla, S. Pöller, Y. Beyl, M. D. Scanlon, S. Beloshapkin, S. Shleev, W. Schuhmann and E. Magner, *Electrochem. Commun.*, 2012, **16**, 92-95.

32. A. W. Zhu, Y. Tian, H. Q. Liu and Y. P. Luo, *Biomaterials*, 2009, **30**, 3183-3188.

33. X. Yang, F. B. Xiao, H. W. Lin, F. Wu, D. Z. Chen and Z. Y. Wu, *Electrochim. Acta*, 2013, **109**, 750-755.

34. S. X. Xu, J. L. Li, Z. L. Zhou and C. X. Zhang, *Anal. Methods*, 2014, **6**, 6310-6315.

35. X. J. Zhao, Z. B. Mai, X. H. Kang and X. Y. Zou, *Biosens. Bioelectron.*, 2008, **23**, 1032-1038.

36. F. H. Wu, Z. C. Hu, J. J. Xu, Y. Tian, L. W. Wang, Y. Z. Xian and L. T. Jin, *Electrochim. Acta*, 2008, **53**, 8238-8244.

37. J. Hong, A. A. Moosavi-Movahedi, H. Ghourchian, A. M. Rad and S. Rezaei-Zarchi, *Electrochim. Acta*, 2007, **52**, 6261-6267.

38. G. Battistuzzi, M. Bellei, C. A. Bortolotti and M. Sola, *Arch. Biochem. Biophys.*, 2010, **500**, 21-36.

39. L. L. Xie, Y. D. Xu and X. Y. Cao, *Colloids Surf. B: Biointerfaces*, 2013, **107**, 245-250.

40. S. Radhakrishnan and S.J. Kim, *RSC Adv.*, 2015, **5**, 12937-12943.

41. U. Salaj-Kosla, S. Pöller, W. Schuhmann, S. Shleev and E. Magner, *Bioelectrochemistry*, 2013, **91**, 15-20.

42. E. Laviron, *J. Electroanal. Chem.*, 1974, **52**, 355.

43. A. I. Gopalan, S. Komathi, G. S. Anand and K. P. Lee, *Biosens. Bioelectron.*, 2013, **46**, 136-141.

44. X. X. Xu, S. Q. Liu and H.X. Ju, *Sensors*, 2003, **3**, 350-360.

45. H. Y. Zhao, Q. L. Sheng and J. B. Zheng, *Microchim. Acta*, 2012, **176**, 177-184.

46. L. Lu, X. R. Huang and Y. B. Qu, *Colloids Surf. B: Biointerfaces*, 2011, **87**, 61-66.

47. L. Lu, Y. Hu, X. R. Huang and Y. B. Qu, *J. Phys. Chem. B*, 2012, **116**, 11075-1080.

48. F. H. Meng, X. L. Yan, J. G. Liu, J. Gu and Z. G. Zou, *Electrochim. Acta*, 2011, **56**, 4657-4662.

49. S. Komathia, A. I. Gopalana, S. -K. Kima, G. S. Anandb and K. -P. Lee, *Electrochim. Acta*, 2013, **92**, 71-78.

50. S. Mao, Y. Long, W. Li, Y. Tu and A. Deng, *Biosens. Bioelectron.*, 2013, **48**, 257-261.

51. Y. Wang, X. Ma, Y. Wen, Y. Xing, Z. Zhang and H. Yang, *Biosens. Bioelectron.*, 2010, **25**, 2442-2446.

52. C. Liu and J. Hu, *Biosens. Bioelectron.*, 2009, **24**, 2149-2154.

Figure captions:

Fig. 1. The fifteenth CV grams of a polished gold electrode in [Choline]Cl·2$ZnCl_2$ at different temperatures (50, 70, 90, 100 and 110 ℃). Scan rate: 0.01 V s^{-1}. Inset: (A) amplified curve from +0.5 V to +0.75 V of the CV gram at 100 ℃ and (B) amplified CV gram obtained at 50 ℃.

Fig. 2. SEM images of the gold electrode after fifty cycles of alloying/dealloying in [Choline]Cl·2$ZnCl_2$ at different temperatures (A-F: 50, 70, 90, 100, 110 and 120 ℃). Inset: EDS spectrum of the surface of NPGE fabricated at 100 ℃. Scan rate: 0.01 V s^{-1}. Scale bars in the SEM images are 100 nm.

Fig. 3. EIS of NPGE (a), HRP/NPGE (b) and Nafion/HRP/NPGE (c) in the aqueous solution of 10 mM $[Fe(CN)_6]^{3-/4-}$ and 0.1 M KCl with the frequencies swept from 10^6 to 10^{-3} Hz at respective open circuit potential.

Fig. 4. CV grams of Nafion/HRP/SGE (a), NPGE (b) and Nafion/HRP/NPGE (c) in 0.1 M phosphate buffer (pH 7.0) at a scan rate of 0.1 V s^{-1}. Inset: the amplified curve a. (Both the SGE and NPGE have the same geometric area.)

Fig. 5. CV grams of Nafion/HRP/NPGE in 0.1 M phosphate buffer (pH 7.0) at different scan rates (a-h: 0.05, 0.10, 0.15, 0.20, 0.25, 0.30, 0.35 and 0.40 V s^{-1}). Inset: anodic and cathodic peak current plotted against the scan rate.

Fig. 6. (A) CV grams of Nafion/HRP/NPGE in 0.1 M phosphate buffer (pH 7.0) in the absence (a) and presence (b) of 0.4 mM H_2O_2 at a scan rate of 0.1 V s^{-1}. (B) Amperometric response of the

smooth gold wire (a) and Nafion/HRP/NPGE (b) toward different H_2O_2 concentrations at -0.02 V in a continuous stirring phosphate buffer. Inset: plot of current responses versus H_2O_2 concentrations.

Fig. 7. Amperometric response of Nafion/HRP/NPGE at -0.02 V in a continuous stirring phosphate buffer (0.1 M, pH 7.0) toward 0.1 mM H_2O_2, 0.2 mM AA, 0.1 mM glucose, and 0.01 mM DA, respectively.

Fig. 1

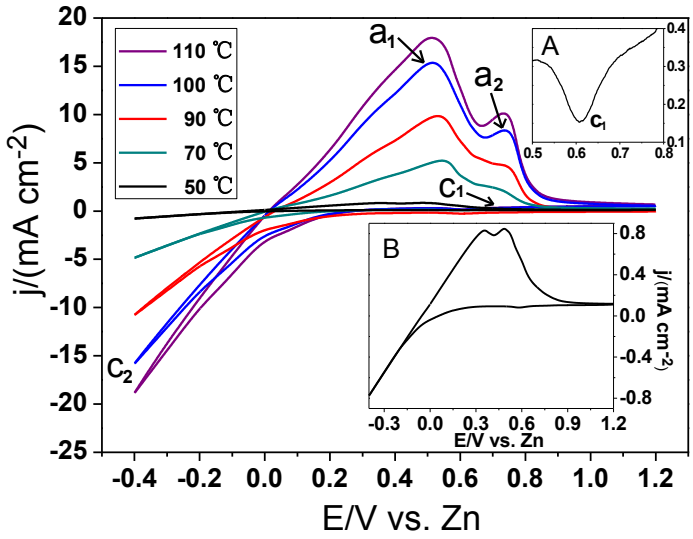

Fig. 2

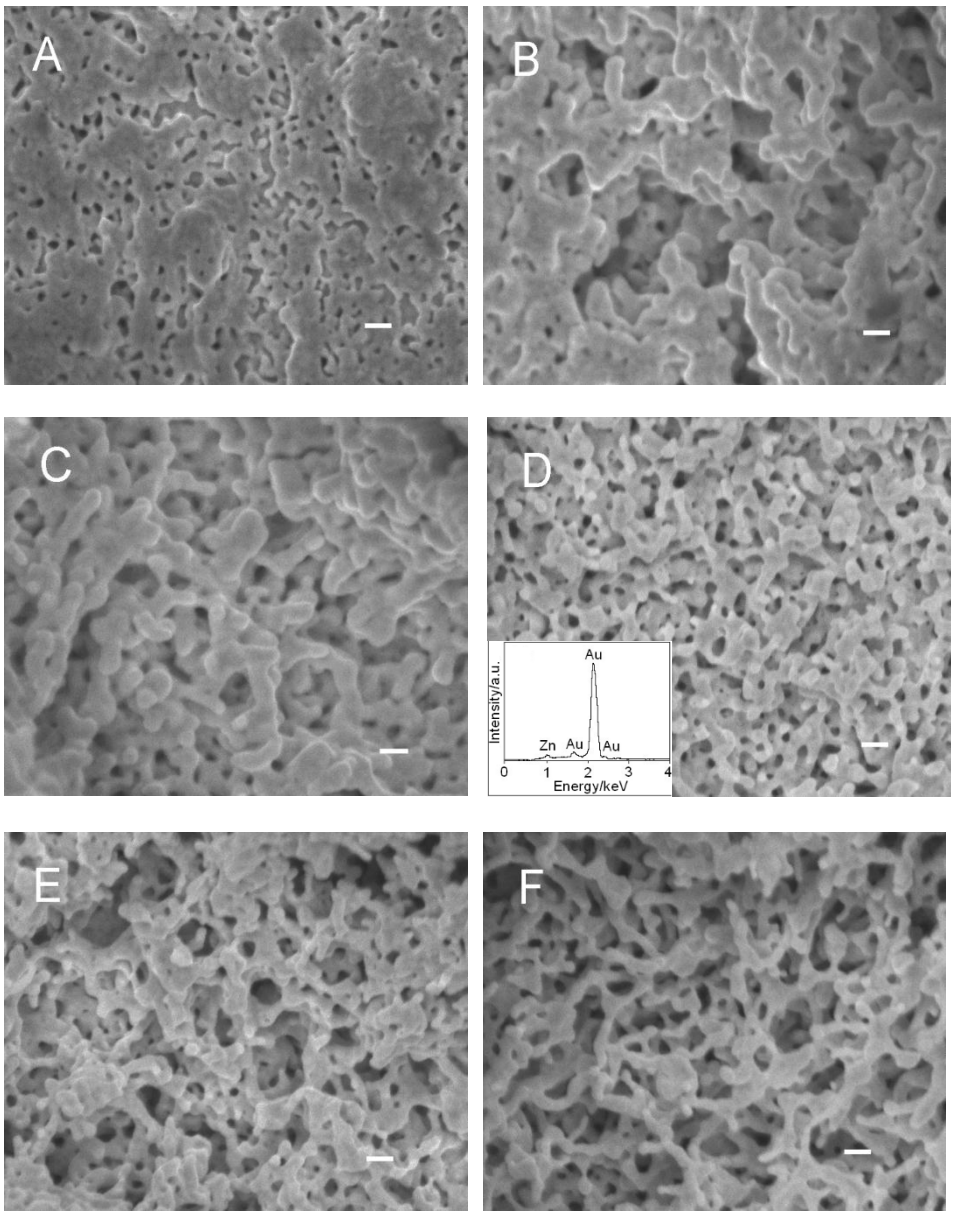

Fig. 3

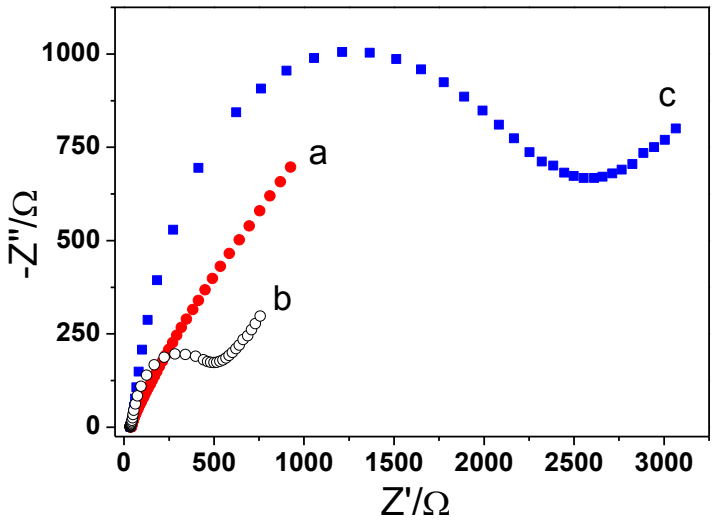

Fig. 4

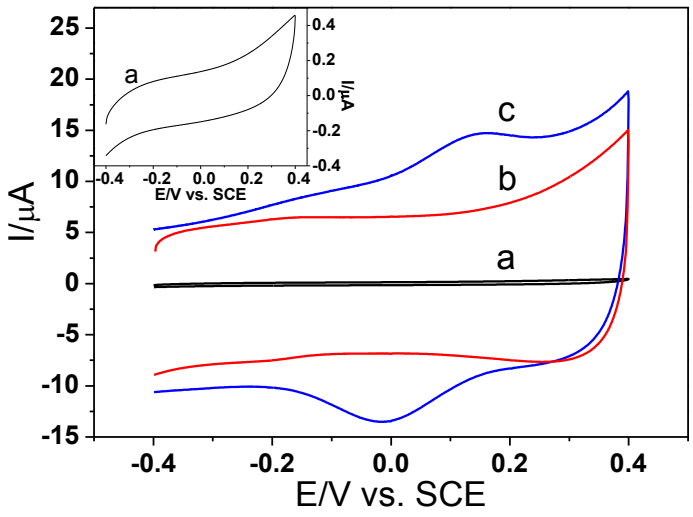

Fig. 5

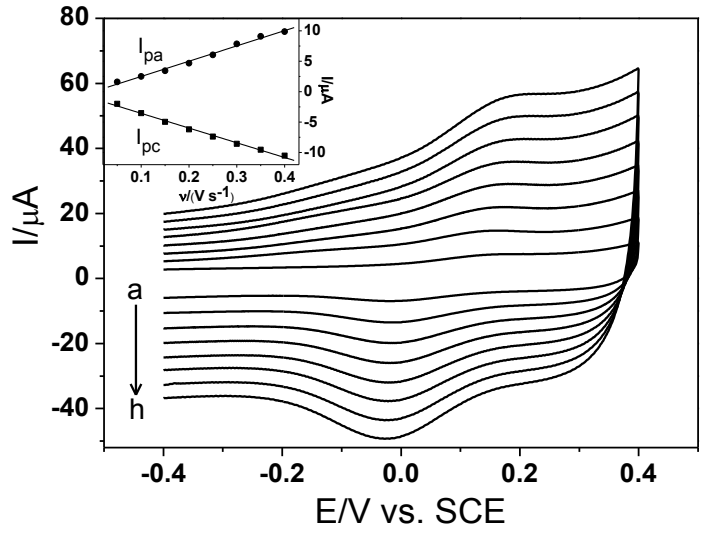

Fig. 6

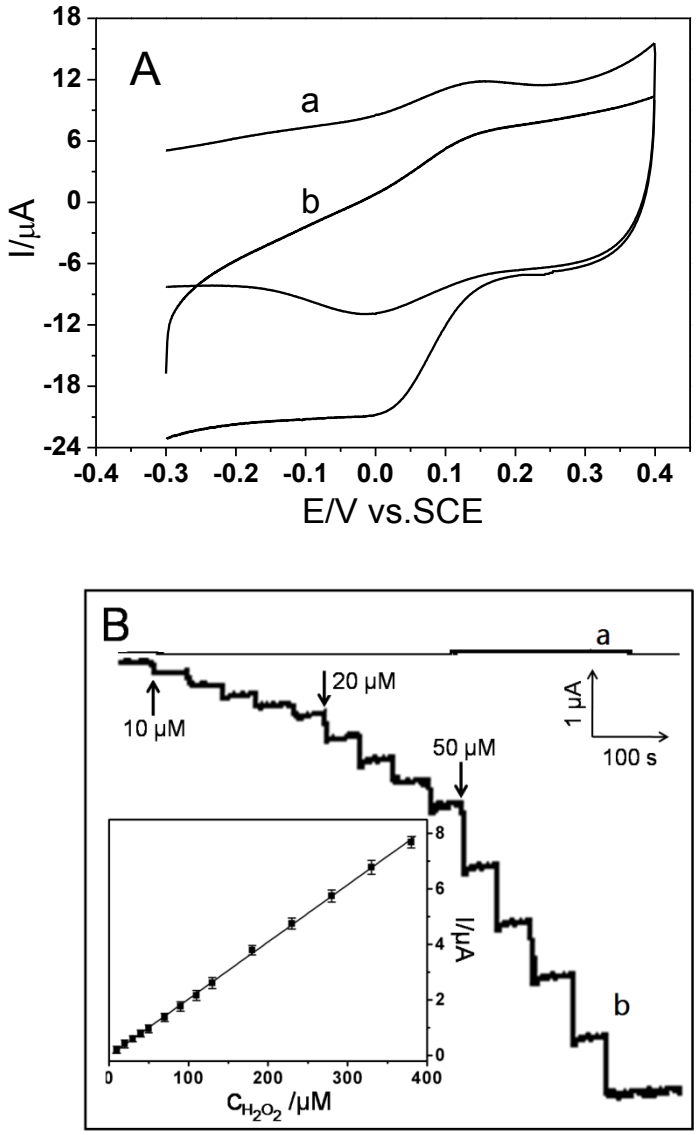

Fig. 7